03,12,13,19

The problems of increasing the thermoelectric figure of merit of polycrystalline misfit layered compounds on $(Gd_xDy_{1-x}S)_zNbS_2$ example

© V.V. Bakovets, A.V. Sotnikov

Nikolaev Institute of Inorganic Chemistry, SB RAS,
Novosibirsk, Russia

E-mail: becambe@niic.nsc.ru

Received October 27, 2022
Revised November 30, 2022
Accepted November 30, 2022

The lattice disorder of different architecture and dimensions influence on the thermoelectric properties (Seebeck coefficient S, resistivity ρ, total thermal conductivity κ_{tot},, power factor S^2/ρ, figure of merit ZT) of the polycrystalline ternary sulfides MTS_3 was studied. The high-temperature misfit layered compounds $(MS)_zNbS_2$ (MS is $Gd_xDy_{1-x}S$ solid solutions) were chosen as objects of the study. The variation of gadolinium concentration along the series $x = 0.0$, 0.1, 0.2, 0.5, 1.0 allowed one to alter the short-range and the long-range order of the crystal lattice and to study their effect on thermoelectric parameters of $(Gd_xDy_{1-x}S)_zNbS_2$. At low concentration of $x = 0.1$ the crystallite size increases, cause the deformation stresses decrease and, thereby, leads to an abnormal changes of S, ρ, κ_{tot} values and ZT decrease. An increase of the gadolinium concentration ($x = 0.2-0.5$) alters the electronic structure and the interatomic bonding character of the incommensurate subsystems $[Gd_xDy_{1-x}S]$ and $[NbS_2]$. In this case, S and ρ values remains practically unaffected, while the thermal conductivity value decreases by 40% and ZT increases by 2 times. The nature of this phenomenon and the anisotropy of the thermoelectric properties were discussed.

Keywords:: misfit layers compounds, thermoelectric properties, lattice disorder, solid solution, crystallite boundaries.

DOI: 10.21883/PSS.2023.02.55889.508

1. Introduction

The considerably increased demand for energy consumption stimulates researchers to develop new effective converter of heat to electric energy. Recovering electric energy from the waste heat loss using thermoelectric materials is considered as one of the most promising method to save the world energy resources [1]. Efficiency of thermoelectric materials is evaluated by the figure of merit:

$$ZT = S^2 \cdot \sigma \cdot T/\kappa_{tot}, \quad (1)$$

where S is Seebeck coefficient, $\sigma = 1/\rho$ is electrical conductivity, κ_{tot} is total thermal conductivity. The search for highly-efficient, cost-effective thermoelectric materials with a high value of ZT is the main problem in the development and application of thermoelectric converters [2–9]. Often the achievement of high ZT value is impeded by the opposite change in parameters S, σ and growth of thermal conductivity κ_{tot} with a change in the chemical composition of materials and an increase in their operating temperature [10]. One of promising solutions of the problem of high ZT achievement is the independent control of electric charges and phonons transfer. The phonon glass-electron crystal (PGEC) concept seems to be a promising strategy to develop thermoelectric materials with high ZT, where the guest (phonon glass) sublattice provides for scattering of phonons and, as a consequence, low κ_{tot}, but at the same time an optimum ratio of S and σ is kept in the host sublattice (electron crystal) [11–13].

Compounds with layer sulfides MTS_3 (where M = Pb, Bi, Sn, Sb, rare earth elements; T = Ti, V, Cr, Nb, Ta) misfit by one of structural parameters ($a_1 \neq a_2$) of sublattices are considered as potential high-temperature thermoelectric materials [14]. These compounds allow realizing the PGEC strategy. The lattices of the CdI_2 „sandwich layer" type of the TS_2-host forms a high mobility of charge carriers. The intercalated lattice of NaCl „double" layer type of the MS-guest and its boundary with the sandwich layer disturb the short-range order and are responsible for the scattering of phonons. For example, value of ZT of the $(La_{1+x}S)_{1.14}NbS_2$ system was improved with a change in concentration of La. An increase in the grain size with increase in the structural order in a sample with $x = 0.05$ have resulted in an increase in power factor (PF) and ZT up to 30% [15]. Regardless, it was found that introduction of Gd^{3+} paramagnetic rare earth ions results in lowering of κ_{tot} in γ-Dy_2S_3 sesquisulfides. Total thermal conductivity of γ-$Dy_{0.8}Gd_{0.2}S_{1.5-y}$ was by 20–25% lower as compared with γ-Gd_2S_3 and by 8% lower than that of γ-Dy_2S_3 [16]. Thus, it is interesting to study the layer sulfide compounds with intercalated layers [LnS] (Ln = lanthanides) [9,14,17] represented by $[Gd_xDy_{1-x}S]$ solid solutions as a guest sublattice in combination with $[NbS_2]$ sublattice as a host.

Since an increase in the ZT parameter requires reduction of thermal conductivity, then it is clear that polycrystal

ceramic thermoelectric materials should be considered more promising, than single-crystal materials due to the increased defectiveness and, as a consequence, the increased scattering of phonons [18–20]. In [21] a significant effect of surface defects on thermoelectric parameters was shown and, in particular, it caused a decrease in thermal conductivity of SnSe(Na,In)-based ceramic materials. Only the grains of microstructure with sizes of about $40\,\mu$m were taken into consideration. However, as it was found in [20], a nanostructured ceramic material with a size of crystallites of $2-80$ nm has lower thermal conductivities at high temperatures. This is explained by the larger specific area of semicoherent boundaries of crystallites and, as a consequence, the considerably higher concentration of defects in the crystal lattice, by ~ 5 orders, than for the boundaries of microstructure grains [22]. In addition, ceramic materials are more manufacturable and cheaper products in the case of wide spreading of thermoelectric converters in the industry and household usage. A typical feature of layer compound ceramics is a set of different types of defects of the long-range and short-range order of the lattice [19,20,23]. These defects include: disordering of solid solutions, cation substitutions, defects of modulated boundaries of misfit lattices, boundaries of crystallites (semicoherent boundaries). A set of such defects provides an opportunity of comparative analysis of the effect of these defects on thermoelectric parameters of materials. Temperature dependencies of thermoelectric and other physical parameters of $(Gd_xDy_{1-x}S)_zNbS_2$ compounds were considered earlier [24,25]. However, the effects of ceramic nanostructure and solid solution composition of the guest sublattice $(Gd_xDy_{1-x}S)$ on thermoelectric parameters S, ρ, κ_{tot} were not analyzed in detail. We have failed to find such an analysis in the literature for other misfit layer compounds as well.

The goal of this work is to study the disturbances of short-range and long-range orders of the crystal lattice arising on the modulated interfaces between misfit sublattices and on crystallite boundaries of ceramic polycrystal materials based on $(Gd_xDy_{1-x}S)_zNbS_2$ compounds with solid solutions in one of the sublattices when their composition is changed, as well as to analyze the mechanisms of charges and heat transfer, which is connected directly to the optimization of thermoelectric parameters S, ρ, κ_{tot} and increase in the ZT quality factor.

2. Experiment

$(DyS)_{1.22}NbS_2$, $(GdS)_{1.20}NbS_2$, $(Gd_{0.1}Dy_{0.9}S)_{1.21}NbS_2$, $(Gd_{0.2}Dy_{0.8}S)_{1.21}NbS_2$, $(Gd_{0.5}Dy_{0.5}S)_{1.21}NbS_2$, and $(GdS)_{0.60}NbS_2$ misfit layer compounds were synthesized. We used Gd_2O_3, Dy_2O_3, and Nb_2O_5 as reagents (all with a purity of 99.99%, by Sibmetalltorg). Details of the experiment and characteristics of samples are reported in the work of [25], which is continued in this study. Seebeck coefficients and resitivity of sintered samples were measured by the simultaneous use of the temperature-differential and the four-probe methods, respectively, on a ZEM-3 system (by Ulvac-Riko, Japan). The total thermal conductivity (κ_{tot}) of each sintered sample was calculated by the ratio of $\kappa_{tot} = DC_pd$, where d, D and C_p — density, thermal conductivity of the sintered sample, and heat capacity of material, respectively. The thermal conductivity was measured on a LFA 457 MicroFlash laser flash system (by Netzsch, Germany) in the range from 300 to 973 K at an Ar flux of $100\,\text{ml}\cdot\text{min}^{-1}$. The heat capacity was determined by indirect method using a LFA 457 instrument with a Pyroceram 9606 reference. Since the Gd, Dy, Nb sulfide-based compounds under study are high-temperature compounds, we analyzed their properties from the point of view of their application as high-temperature thermoelectric materials. Therefore, this work presents the results of analysis of S, ρ and (S^2/ρ) dependencies on the composition of xGd solid solution of the $[Gd_xDy_{1-x}S]$ sublattice mainly for a temperature of 873 K and partially, for comparison, for a temperature of 300 K, where it is necessary. In the temperature range of $300 < T < 873$ K, thermoelectric parameters S, ρ and κ_{tot} had intermediate values and no qualitative features of their change with the composition of $[Gd_xDy_{1-x}S]$ sublattice were found. Therefore, the consideration of these parameters was omitted.

3. Results and discussion

3.1. XRD-analysis

Fig. 1 shows x-ray patterns of powders of $(DyS)_{1.22}NbS_2$, $(Gd_{0.1}Dy_{0.9}S)_{1.21}NbS_2$, $(Gd_{0.2}Dy_{0.8}S)_{1.21}NbS_2$, $(Gd_{0.5}Dy_{0.5}S)_{1.21}NbS_2$, and $(GdS)_{1.20}NbS_2$ layer

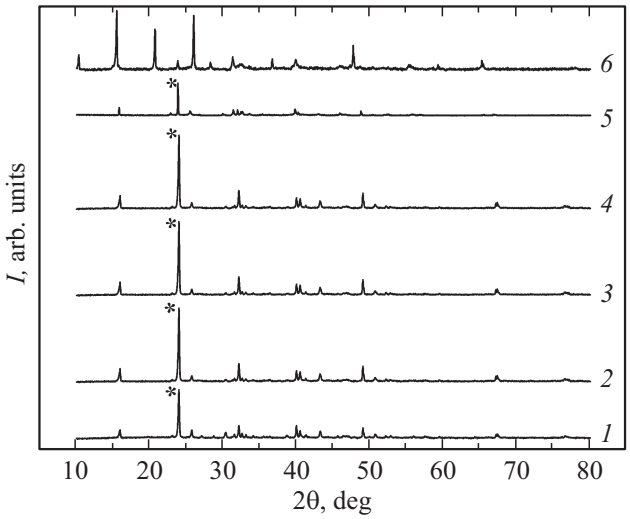

Figure 1. XRD-powder patterns of sintered samples: $(DyS)_{1.22}NbS_2$ — *1*, $(Gd_{0.1}Dy_{0.9}S)_{1.21}NbS_2$ — *2*, $(Gd_{0.2}Dy_{0.8}S)_{1.21}NbS_2$ — *3*, $(Gd_{0.5}Dy_{0.5}S)_{1.21}NbS_2$ — *4*, $(GdS)_{1.20}NbS_2$ — *5* and $(GdS)_{0.60}NbS_2$ — *6*. Plane (006) is marked with asterisk.

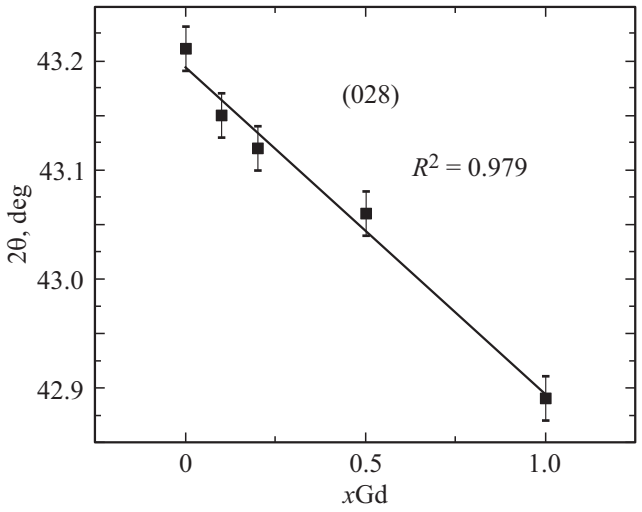

Figure 2. The dependence of change in the position of diffraction peak maximum at $2\theta \sim 43$ deg on the composition of xGd. The index of (028) plane is corrected in relation to the data reported in [29] taking into account the ICSD international database (ICSD № 75444).

compounds. All synthesized compounds with $(Gd_xDy_{1-x}S)$ have the same crystal structure as reference compounds $(DyS)_{1.22}NbS_2$ and $(GdS)_{1.20}NbS_2$ [17,26–28].

Diffraction peaks of $(Gd_xDy_{1-x}S)_zNbS_2$ compounds shift toward smaller 2θ angles by 0.15−0.25 deg with an increase in the concentration of xGd up to $x = 1$ [29,30], which is related to the smaller radius of Dy^{3+} ions (0.105 nm) as compared with Gd^{3+} (0.115 nm) with the coordination number of cations equal to 6 [31]. No changes were observed in positions of diffraction peaks with a change in x in the range of 0.0−0.1 and in some cases up to 0.2 for angles $2\theta \sim 15.90$, 23.90, 32.10, 40.00, 40.50, and 49.00 deg. At $x\text{Gd} > 0.2$ peaks had a monotonous shift toward lower 2θ for $(GdS)_{1.20}NbS_2$. These features are related to the redistribution of cations over modulated interfaces of sublattices $[Gd_xDy_{1-x}S]$ and $[NbS_2]$ and over boundaries of crystallites [14,29,30]. There are three possible causes for the absence of shift of diffraction peaks in the region of low concentrations of Gd^{3+} ions $(x = 0.0-0.2)$:

– some diffraction peaks are related to the more stable sublattice of the sandwich $[NbS_2]$, because Ln^{3+} ions are not included in this sublattice [14],

– Gd^{3+} ions are positioned in a disordered manner over misfit modulated guest−host interfaces of $(00l)$ sublattices,

– Gd^{3+} ions are surface-active ions and anisotropically localized on crystallite boundaries along appropriate planes (hkl). Their concentration inside crystallites is less than that set by the composition (Gd_xDy_{1-x}).

Only the dependence of $2\theta = f(x)$ at $2\theta \sim 43.00$ deg is described by the Vegard's law (Fig. 2) with a squared regression coefficient of $R^2 = 0.979$ in the whole range of x and, hence, the corresponding diffraction peak can probably be considered as related to the [LnS] sublattice. No peak is observed at $2\theta = 43.00$ deg in Fig. 1 due to the low intensity, however it is shown in the table of obtained diffraction patterns.

Fig. 3 shows two projections of the (028) plane in the orthorhombic layer structure of $[Gd_{0.957}S]$ sublattice of the compound with $[CrS_2]$ sandwich close to the structural analogue of the layer compound with $[NbS_2]$ [14]. In the $(DyS)_{1.22}NbS_2$ compound, the unit cell of the [DyS] sublattice is monoclinic [14]. Parameters of the unit cell (UC) $a_1 = 5.4126$ Å, $b_1 = 5.6722$ Å and $c_1 = 22.2794$ Å almost completely coincide with those for the orthorhombic cell of the [GdS] sublattice in the $(GdS)_{1.27}CrS_2$ related compound ($a_1 = 5.4541$ Å, $b_1 = 5.8098$ Å and $c_1 = 21.461$ Å). However, an insignificant difference of 0.319° can be noted in β angles (see ICSD 75444). Thus, it can be taken that the (028) plane for the investigated compounds has nearly identical orientation in relation to **a, b, c** vectors, as well as for $(GdS)_{1.27}CrS_2$. We have failed to find a closer structural analogue in the ICSD database.

The (028) plane intersects the (006) basal plane along the row of cations of the $[Gd_xDy_{1-x}S]$ sublattice with a shift along the a axis. Thus, it can be assumed that interstitial Gd^{3+} ions at a low concentration replaces the Dy^{3+} ions in positions of the highest bond energy (coherent positions) with S^{2-} ions of the $[NbS_2]$ sublattice. These are the positions, that are the most ordered on the guest−host interface, because they obey the structure of misfit layer compounds defined by the modulation parameter $q = a_1/a_2$ [17], where a_1 and a_2 — parameters of the UC of sublattices.

Thus, the analysis of the change in positions of diffraction peaks indicates that there is a trend to form a solid solution in the $[Gd_xDy_{1-x}S]$ subsystem. However, these solid solutions are strongly disordered.

3.2. Morphological and structural disordering of crystallites

In addition to above-mentioned structural features of misfit layer compounds, other defects exist in the ceramic samples as well, such as: vacancies, dislocations, and deformation centers caused by the presence of semicoherent boundaries of crystallites [24,32–34]. These boundaries are characterized by small tilt angles of crystal lattices in relation to each other with formation of edge dislocations (Fig. 4).

Based on X-ray patterns, effective values of coherent scattering regions were calculated (CSR_{H-W}) equivalent to the sizes of crystallites (D_{H-W}) after the deformation component is deduced. For this purpose we used the Williamson−Hall plot analysis method [35,36] (Fig. 5, *a*). Knowing D_{H-W}, we determined the specific area of crystallite boundaries (S_{cr}) (specific area of boundaries per $1\,cm^3$) in the isometric approximation of prismatic crystallites. The formation of these boundaries is accompanied with formation of a network of dislocations. Dislocations are energy-strong defects that deform the lattice [36–38]. The deformations decrease in inverse proportion to the

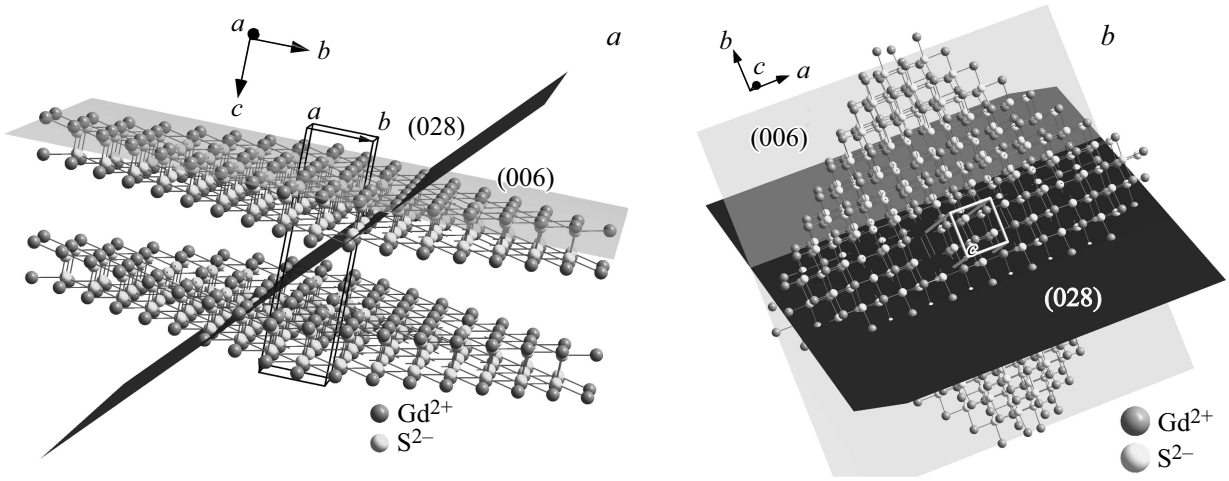

Figure 3. Orthorhombic sublattice [GdS] in the $(Gd_{0.96}S)_{1.27}CrS_2$ compound: projection **a** — (*a*) and **c** — (*b*).

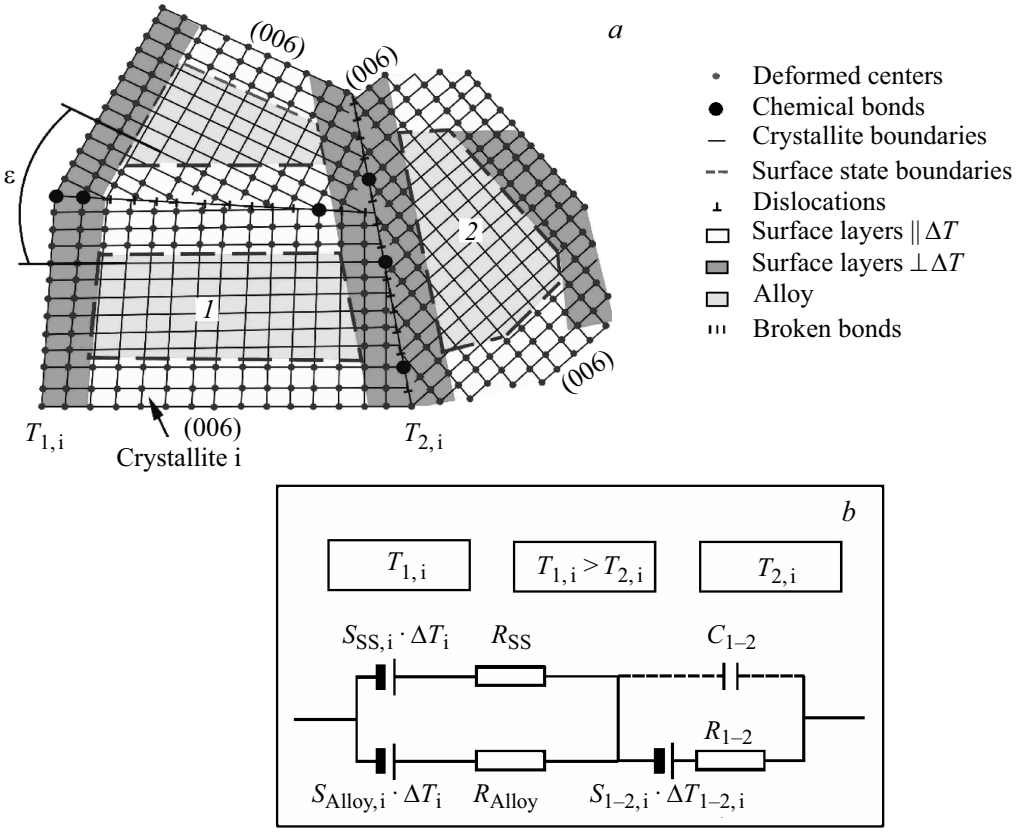

Figure 4. Semicoherent boundaries with edge dislocations between neighbor crystallites — (*a*), equivalent electric circuit diagram of crystallite — (*b*).

distance r from the dislocation $(1/r)$. The number of atoms per unit area of crystallite boundaries is $\sim 2 \cdot 10^{14}\,\mathrm{cm}^{-2}$. It is known that deformation stresses decrease by an order of magnitude at a distance of 10 atomic layers [37,38]. Thus, a semicoherent boundary and 5 atomic layers parallel to it on both sides are severely disturbed. Then the number of deformed centers of the lattice N_{cr} related to the presence of semicoherent boundaries of crystallites can be determined using the following relationship $N_{cr} = 2 \cdot 10^{14} S_{cr}$. With $D_{H-W} = 90\,\mathrm{nm}$ N_{cr} achieves a value of $1.3 \cdot 10^{21}\,\mathrm{cm}^{-3}$ [29]. Fig. 5 shows dependencies of crystallite sizes and specific concentration of deformed centers of the crystallite lattice on the composition of the solid solution sublattice $(Gd_xDy_{1-x}S)$. Compounds with a composition of $(Gd_{0.1}Dy_{0.9}S)_{1.21}NbS_2$ are characterized by the presence of anomalous changes N_{cr}.

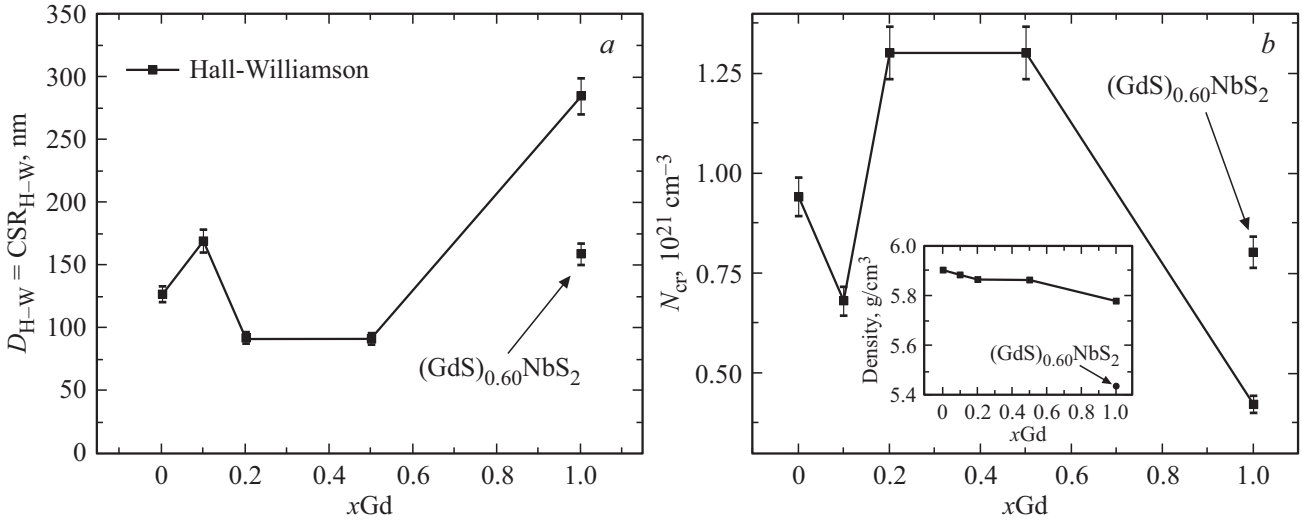

Figure 5. Dependencies of D_{H-W} — (*a*) and N_{cr} — (*b*) on *x*Gd (insert: densities of the compounds under study).

It is clear that values of N_{cr} are quite high and have specific dependencies on the composition of the *x*Gd solid solution and are inversely proportional to the change D_{H-W}.

3.3. Features of the change in electric parameters of ceramic samples

In accordance with the nature of uniaxial compression of powders of layer compounds, the developed planes of lamellar crystallites and grain boundaries (of aggregated crystallites) are oriented with some deviation in the plane of pressure [14,39]. In this case this plane is the (006) plane. Indices in and out used are referred to physical parameters in the directions parallel (in-plane) and perpendicular (out-of-plane) to the plane of pressure during formation of the ceramic samples. Fig. 6, *a, b, c* shows dependencies of S_{in}, S_{out}, ρ_{in}, ρ_{out}, and $(S^2/\rho)_{in}$, $(S^2/\rho)_{out}$ on the composition of *x*Gd solid solution of $[Gd_xDy_{1-x}S]$ sublattice in ceramic samples of layer compounds in question for temperatures of 873 and 300 K. As can be seen, the anisotropy of these parameters is clearly manifested.

For the samples of compounds with the $[NbS_2]_2$ two-layer sandwich, the anisotropy of these parameters is weakly manifested. As it was shown, in this case the long-range and short-range orders of the structure were relatively severe disordered according to the data of XRD, which also follows from the analysis of the data of Raman scattering spectroscopy of light [29].

For the sample of $(Gd_{0.5}Dy_{0.5}S)_{1.21}NdS_2$ the Seebeck coefficient S_{in} increases from $\sim 30\,\mu V \cdot K^{-1}$ at 300 K to $\sim 77\,\mu V \cdot K^{-1}$ at 873 K, and ρ_{in} increases from $\sim 6\,\mu\Omega \cdot m$ at 300 K to $\sim 17\,\mu\Omega \cdot m$ at 873 K. Sign of *S* is positive, that confirms the semiconductor conductivity of *p*-type. All samples demonstrate anisotropic *S* and ρ in the whole range of *x*Gd compositions. Values of *S* and ρ are almost constant with increase in the concentration of *x*Gd. However, with a low concentration of $x\text{Gd} = 0.1$ anomalous changes in the investigated parameters are observed $S_{in} > S_{out}$ at temperatures of 873 and 300 K. For single crystals of degenerate semiconductors (parabolic band, approximation of inelastic scattering), including the misfit compounds, value of *S* is defined by equation (2) [10]:

$$S = \frac{8 \cdot \pi^2 \cdot m^* \cdot k_B^2 \cdot T}{3p^+ \cdot h^2} \cdot \left(\frac{\pi}{3n}\right)^{2/3}, \qquad (2)$$

where k_B — Boltzmann constant, m^* — effective mass of charge carrier, *T* — temperature in Kelvin degrees, *h* — Planck constant, p^+ — hole charge, *n* — concentration of charge carriers. This relationship should be used with care to determine m^* in different direction of anisotropic crystal structures. For example, this relationship was used in [15] to determine the ratio of effective masses m^*_{in} and m^*_{out} of holes from the ratio of experimental values of $S_{in} > S_{out}$ for ceramic anisotropic materials. As a result, the following relationship was obtained: $m^*_{in} \sim 2m^*_{out}$ at $S_{in} > S_{out}$. However, for an estimate like this it is necessary to take into account the anisotropy of physical properties of layer materials, such as $(LnS)_z NbS_2$, and features of the internal morphology of ceramic samples. First, for intercalated anisotropic structures with a thickness of layers of [LnS] and $[NbS_2]$ sublattices at the level of a few atomic distances there is no data on the ratio of lengths and times of free paths of charge carriers, as well as on their mobilities, and quantum-mechanical calculations have yielded contradictory conclusions on the presence or absence of anisotropy of the electron structure of bands [15,40] in in-plane and out-of-plane directions of the structure. It is clear that such calculations do not take into account a number of defects of short-range and long-range orders of the lattice of real polycrystal samples. Second, the packing of layer crystallites in polycrystal ceramic materials has little, yet noticeable deviations from the *c* crystallographic direction

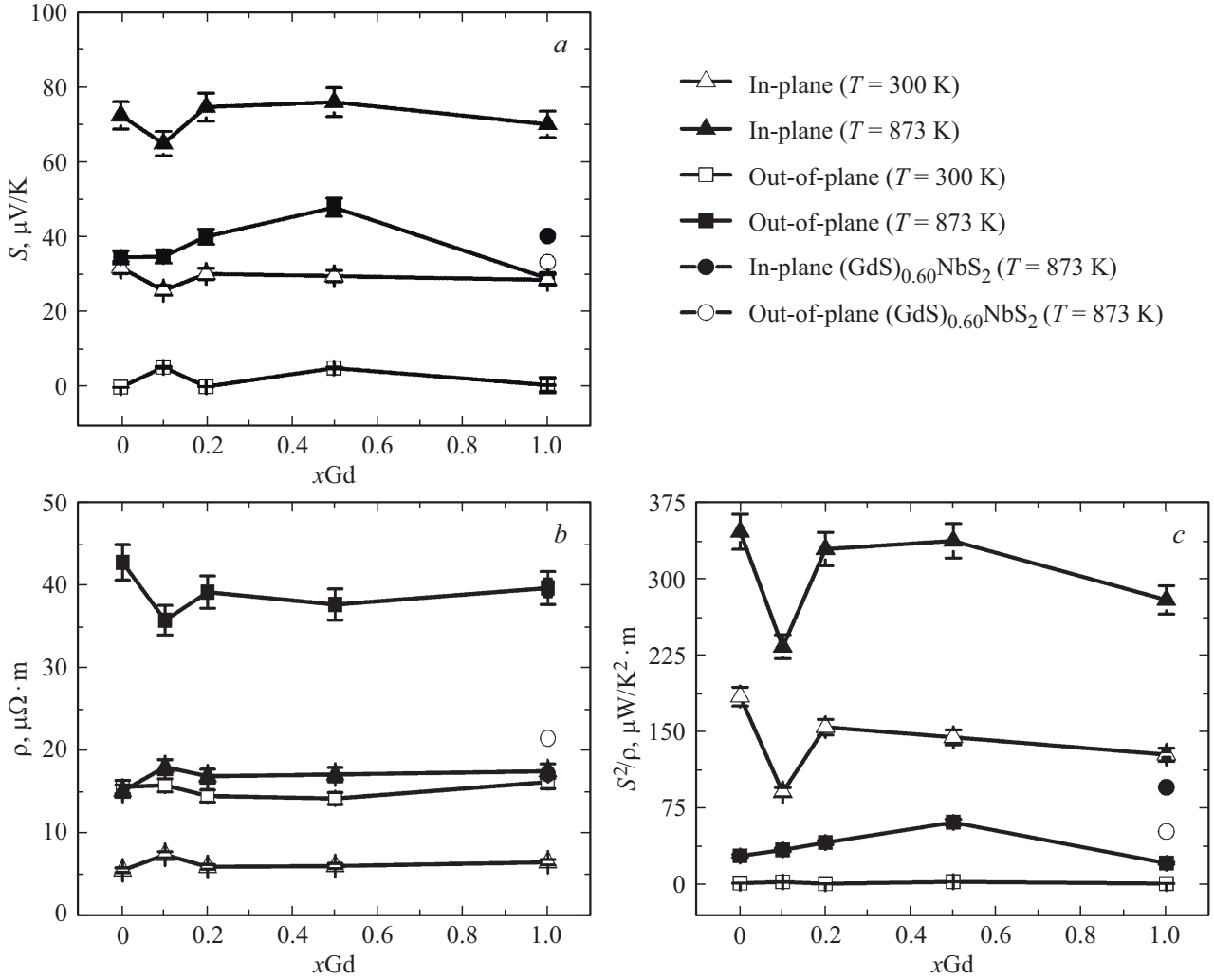

Figure 6. Seebeck coefficients S in (in-plane) and (out-of-plane) directions — (a), resitivity ρ — (b), thermoelectric power factor S^2/ρ — (c) as a function of content of xGd in $(Gd_xDy_{1-x}S)_zNbS_2$ at room temperature and at 873 K.

of crystallites [15], which will cause a partial superposition of projections of in and out components of crystallite parameters on in-plane and out-of-plane directions of the ceramic sample in general, making difficult physical interpretation of these parameters [10,40]. Also, the interpretation of results becomes difficult because nothing is known about the complexity of the structure of electron bands in these directions [41]. Third, there is no information about values of effective masses of charge carriers on the boundaries of contacting crystallites in in- and out-of-directions. Thus, the most likely is that the values obtained in the above-mentioned studies are superpositions of projections of m^*_{in} and m^*_{out} of charges in layer compounds on the temperature gradient direction under consideration in the sample. Hence, the values of m^*_{in} and m^*_{out} determined in the above-mentioned and similar works on the calculation of effective masses of charge carriers using equation (2) can not be used to explain the nature of charge carriers transfer in the field of temperature gradient for the pressed ceramics of misfit layer compounds. Traditionally, the effective masses of carriers are measured by the method of cyclotron resonance on single crystals and other spectroscopic methods.

At $x = 0.1$ an anomalous change in both the S and the ρ takes place. S_{in} decreases from ~ 73 to $\sim 65\,\mu V \cdot K^{-1}$, while ρ_{in} increases from ~ 15 at $x = 0$ to $\sim 19\,\mu\Omega \cdot m$ (at 873 K). However, ρ_{out} decreases, which correlates with the increase in crystallinity of samples. The increase in crystallinity of the $(Gd_{0.1}Dy_{0.9}S)_{1.21}NbS_2$ lattice is confirmed by a decrease in specific area S_{cr} of crystallite boundaries and, respectively, a decrease in concentration of deformation centers of the lattice (Fig. 5, b). It follows therefrom that gadolinium is a surface-active substance (SA) and a promoter of crystallite growth. At a low concentration in the system gadolinium is concentrated near semicoherent boundaries of crystallites. The phenomenon of atomic SA impurities concentrating near crystallite boundaries was demonstrated many times before [18 and others]. Moreover, cations of the $Gd^{(2\div3)+}$ impurity replace the $Dy^{(2\div3)+}$ cations in positions adjacent to cation vacancies of $[V_{Dy}]$, because volume of the $Gd^{(2\div3)+}$ ion is greater than

that of the $Dy^{(2\div3)}$ ion. The presence of cation vacancies $[V_{Ln}]$ is a normal phenomenon for $(LnS)_zNbS_2$ [15,42] misfit layer compounds and inherent to solid solutions in general, especially on crystallites boundaries. As a result, the content of gadolinium ions in the volume of crystallites appears to be less than it is defined by the stoichiometry of the solid solution based on the concentration of initial reagents. This is reflected in the unchanged position of some reflections on x-ray patterns through to compositions of $x\mathrm{Gd} \geq 0.2$ [29]. The electron and phonon structures of the under-study misfit layer compounds with solid solutions in the $[Ln(1)_xLn(2)_{1-x}S]$ guest sublattice at xGd from 0.0 to 0.1 change quite noticeably. Indeed, we observed it by an anomalous decrease in the bandgap on diffusion reflection spectra and by a change in RSS spectra (Raman scattering spectra) [29]. In addition, it is found that with substitution of $Dy^{(2\div3)+}$ ions by $Gd^{(2\div3)+}$ ions in the $[Gd_xDy_{1-x}S]$ sublattice, distances between atoms of Dy and atoms of S of $[NbS_2]$ sandwiches decrease in accordance with the results of EXAFS-spectroscopy [29]. Also, anomalies in the electron structure were observed with a change in the stoichiometry of $(La_xS)_{1.14}NbS_2$ misfit compounds with $x = 0.95,\ 1.00,\ 1.05$ [15]. These effects are explained by the change in concentration of charge carriers, i.e. holes, the limited motion of holes in double layers of [LnS], the anomalous scattering of charge carriers on the modulated interfaces between the layers of $[Gd_xDy_{1-x}]$ and $[NbS_2]$ of sublattices due to the occurrence of anharmonicity of the lattice [14,22,43].

With an increase in concentration of xGd from 0.1 to ≥ 0.2 the $Dy^{(2\div3)+}$ ions are replaced by $Gd^{(2\div3)+}$ ions in the $[Gd_xDy_{1-x}S]$ sublattice in non-coherent nodes of modulated interface between the layers of sublattices forming a solid solution close to the ordered one. Indeed, the majority of x-ray reflections (hkl) are shifted monotonously and in a manner close to the Vegard's law toward their position in the structure of $(GdS)_{1.20}NbS_2$ compound. At the same time the short-range and long-range orders on the interface between $[Gd_xDy_{1-x}S]$ and $[NbS_2]$ sublattices increase up to $x = 0.2$ and then remain unchanged in the range of $x\mathrm{Gd} = 0.2{-}0.5$ (Fig. 5, *b*). These effects are accompanied with an increase in S_{in}, S_{out}, and ρ_{out}, and for $x\mathrm{Gd} > 0.2$ the S and ρ parameters remain almost constant, except for S_{out}.

The resitivity of the crystallite of misfit layer compounds, taking into account the change in solid solution composition in the $[Gd_xDy_{1-x}S]$ sublattice, can be represented by developing the model proposed for single crystals [44–48] as follows:

$$\rho_{cr,out} \approx \rho_{[Gd,DyS],out} + \rho_{[NbS2],out},$$

$$\rho_{cr,in} \approx (\rho_{res} + \rho_{Ph} + \rho_{\mu,eff})_{[Gd,DyS],in} \times \rho_{[NbS2],in} \Big/ \left[(\rho_{res} + \rho_{Ph} + \rho_{\mu,eff})_{[Gd,DyS],in} + \rho_{[NbS2],in}\right],$$

$$\rho_{[NbS2],in,out} = 1/np^{+}\mu_{h,in,out}, \qquad (3)$$

where $\rho_{[Gd,DyS]}$ and $\rho_{[NbS2]}$ — resitivitys of layers of $[Gd_xDy_{1-x}]$ and $[NbS_2]$ sublattices, ρ_{res} — temperature-independent resitivity due to lattice defects, ρ_{Ph} — scattering of charges on phonons, $\rho_{\mu,eff}$ — scattering of charges on local magnetic moments. The last term is low in the range of $x\mathrm{Gd} = 0.2{-}0.5$, because the effective magnetic moment μ_{eff} of the compounds in question is low and almost constant [29], n — number of charge carriers, p^+ — charge of carriers, μ_h — mobility of holes, $\rho_{[NbS2]}$ remains almost constant since Ln^{3+} ions do not implant into the $[NbS_2]$ sandwich. ρ_{Ph} can increase slightly according to the Raman scattering spectra in the range of $x\mathrm{Gd} = 0.2{-}0.5$ as the density of phonon states increases and the symmetry of terms becomes disturbed. In addition, $\rho_{res,in}$ and $\rho_{res,out}$ of $[NbS_2]$ layers remain nearly constant with a change in xGd, because almost equal number of electrons of Gd ions (0.82e-/Nb) and (0.83e-/Nb) of Dy ions transit to the band d_{z2} of Nb^{4+} ion of the electrically conductive $[NbS_2]$ sandwich in accordance with [45,46]. Since sizes of Dy^{3+} and Gd^{3+} ions are close to each other [31], all terms of resitivitys of [Gd, DyS] should be almost constant in equations (3) in the range of $x = 0.2{-}0.5$. It was obtained experimentally for the single crystal, that $\rho_{in} \ll \rho_{out}$ [44] due to the effect of the structural anisotropy. In our case, for polycrystal samples a lower ratio of $\rho_{in} < \rho_{out}$ (Fig. 6, *b*) was obtained. At the same time, an anomaly of absolute values of ρ_{in} and ρ_{out} occurs at a low concentration of $x\mathrm{Gd} = 0.1$. These effects are related to the above-mentioned noticeable deviations of orientation of crystallites and their aggregates in the ceramic sample from the crystallographic axis c and to the changes in concentration of lattice defects with a change in specific area of crystallite boundaries.

The resitivity ρ_{in} of the $(GdS)_{0.60}NbS_2$ compound with double $[NbS_2]_2$ layer remains almost unchanged, so $\rho_{in,(GdS)_{0.60}NbS2} \sim \rho_{in,(GdS)_{1.20}NbS2}$. Similar results were obtained on single crystals at ~ 300 K [14,44]. On the other hand, $\rho_{out,(GdS)_{1.20}NbS2}$ is higher than $\rho_{out,(GdS)_{0.60}NbS2}$ due to the higher number of semicoherent boundaries of $[GdS]{-}[NbS_2]$ per unit length of the sample.

Equations (3) are referred to single crystal or, in our case, to the volume part of one crystallite. In the case of polycrystal samples, it is necessary to take into account the charge transfer along the boundaries and normal to the boundaries of crystallites in the direction of temperature gradient. The analysis of this complex process is based on the equivalent electric circuit diagram of one crystallite (Fig. 4, *b*) taking into account surface phenomena in the case of charge transfer in the direction of temperature gradient, which is described by the following equations:

$$R_{cr,i} = R_{eff,i} + R_{1-2,i}$$

$$R_{eff,i} = R_{Alloy,i} \cdot R_{SS,i}/(R_{Alloy,i} + R_{SS,i}),$$

$$E_{cr,i} = \int_{\Delta T_i} f\left[S_{Alloy,i}(T), S_{SS,i}(T)\right]dT + \int_{\Delta T_i^*} f\left[S_{1-2i}(T)\right]dT \qquad (4)$$

where: $R_{cr,i}$ — resistance of the i-th crystallite parallel to the direction of temperature gradient ΔT_i, $R_{eff,in}$ — total resistance of the volumetric part of crystallite and its side boundaries $R_{SS,i}$ parallel to the temperature gradient ΔT_i, $R_{(1-2),i}$ — resistance of the layer at the semicoherent boundary $(1-2)$ of adjacent crystallites normal to the temperature gradient ΔT_i^*, $R_{Alloy,i}$ — resistance caused by the scattering of charge carriers on the lattice and defects, R_{SS} — resistance of layers of semicoherent side boundaries parallel to ΔT_i, E_i — thermo-emf (EMP) at the i-th crystallite in the regions of temperature gradients ΔT_i and ΔT_i^*, $S_{Alloy,i}(T)$, $S_{SS,i}(T)$ and $S_{1-2,i}(T)$ — temperature dependencies of Seebeck coefficients for the crystallite volume, side boundaries, and the layer of semicoherent boundary $(1-2)$, respectively, in the direction parallel to ΔT. $R_{Alloy,i}$, $R_{SS,i}$, and $R_{1-2,i}$, essentially the internal resistances of EMP sources, are connected in parallel/in series and at certain ratios depending on temperature conditions can couple each other. It is clear, that when evaluating the thermoelectric figure of merit of a material by equation (1), the resistivity of crystallite $\rho_{cr,i}$ can be taken as $R_{cr,i} \cdot l_{cr,i}$, where $l_{cr,i}$ being length of the crystallite in the direction of ΔT_i, since $l_{cr,i} \gg h_{1-2,i}$, where $h_{1-2,i}$ is thickness of the deformed layer of the adjacent crystallites boundary. This will be true also for the whole homogeneous real sample in the case of the same chemical and phase compositions of crystallites and their mean sizes equal to each other.

$f[S_{Alloy,i}(T), S_{SS,i}(T)]$ and $f[S_{1-2,i}(T)]$ functions are complex, currently not described, their form being dependent on the concentration of charge carriers n_h, their effective masses $m^*_{eff,h}$, and structure of electron bands in the appropriate regions of the crystallite (volume, boundaries). To evaluate ZT, the value of $S_{cr,i}$ can be taken as $E_{cr,i}/\Delta T_i$, since $\Delta T_i \gg \Delta/T_i^*$.

Thus, it is necessary to emphasize that to solve successfully the material engineering problem of effective thermoelectric ceramic materials creation, a theoretical analysis and experimental verifications of the form of $f[S_{Alloy,i}(T), S_{SS,i}(T)]$ and $f[S_{1-2,i}(T)]$ functions, $R_{Alloy,i}$, $R_{SS,i}$, and $R_{1-2,i}$ parameters and their temperature dependencies are needed for the required temperature range of application of the thermoelectric materials, which are promising by their preliminary parameters. At the same time, of course, it is necessary to take into account features of temperature dependencies of κ_{tot}, $\kappa_{e,h}$ (heat transfer by charge carriers drift) and κ_{lat} (heat transfer by phonons of real lattice taking into account the effect of defects of the short-range and long-range orders) parameters.

The following effects can occur in different thermoelectric materials on semicoherent boundaries of crystallites and their surfaces, which are especially significant for certain compositions and structures of materials, that must be taken into account for polycrystal ceramic samples [47,48]:

– formation of Tamm and Shockley surface states with a concentration of up to $10^{12}-10^{15}\,cm^{-2}$, as well as on defects and impurities of SAs,

– occurrence of a spatial charge region on boundaries of neighbor crystallites with sufficient chemical or structural heterogeneity, when barrier layers can be formed and $R_{(1-2)}$ can increase,

– co-existence of surface states with different relaxation times: fast $10^{-12}-10^{-6}$ s, intermediate $10^{-6}-10^{-3}$ s, slow $> 10^{-3}$ s,

– occurrence of a barrier layer between neighbor crystallites in the direction of temperature gradient can form a capacitance reactance of $C_{(1\text{-}2),i}$ (see Fig. 4, *b*), overcoming of which will be related to a heat emission, tunnel currents, or a diffusion transfer,

– with low concentrations of one of components, for example $x\mathrm{Gd} = 0.1$ in our case, the above-mentioned effects can have an anomalous change due to the increased concentration of this component on boundaries of crystallites as a surface-active substance (SA),

– occurrence of a band-bending on boundaries of crystallites in a semiconductor.

At the same time mobility of charges can change by an order of magnitude, as well as the following can change: relationships of $R_{Alloy} < R_{SS}$ or $R_{Alloy} > R_{SS}$, as well as enriched or inverted layers can arise with corresponding values of S_{SS}; at the same time boundaries of opposite conductivity type can be formed. For example, this phenomenon is recorded on single crystal Si and Ge diodes [49], and these materials are widely used as thermoelectrics as well [20,50,51]. The anisotropy of conductivity with a change in sign of the S parameter was also observed for layer compounds [52].

The power factor (PF) changes with increase in the concentration of xGd. Absolute values (S^2/ρ) for all studied compounds in the in-plane direction of samples are higher than in the out-of-plane direction. PF at $x = 0.1$ is the lowest, and at $x = 0.0$ and 0.5 it is the highest for the investigated compounds. PF for the $(GdS)_{0.60}NbS_2$ compound is very low and almost the same for the in-plane and out-of-plane directions. Since the power factor S^2/ρ is considerably higher for the in-plane direction, it is reasonable to consider the nature of thermo-emf (EMP) formation and charge transfer in the polycrystal ceramic materials in the field of temperature gradient for this direction, bearing in mind the goal to produce a material with improved thermoelectric efficiency.

3.4. Change in the thermal conductivity

Dependencies of κ_{tot} on concentration of xGd are shown in Fig. 7, *a*. Behavior of these dependencies repeats the behavior of the $CSR = f(x)$ dependence (Fig. 5, *a*) with an anomalous change at $x = 0.1$. At the same time the sequence of shift of the $\kappa_{tot,in}$ dependence on temperature with a change in composition is disturbed significantly for the sample with $x = 0.1$ (Fig. 7, *b*). The degree of long-range and short-range orders for the $(GdS)_{1.20}NbS_2$ compound (Fig. 5, *a, b*) is considerably higher than that for the $(GdS)_{0.60}NbS_2$ compound due to the fact that

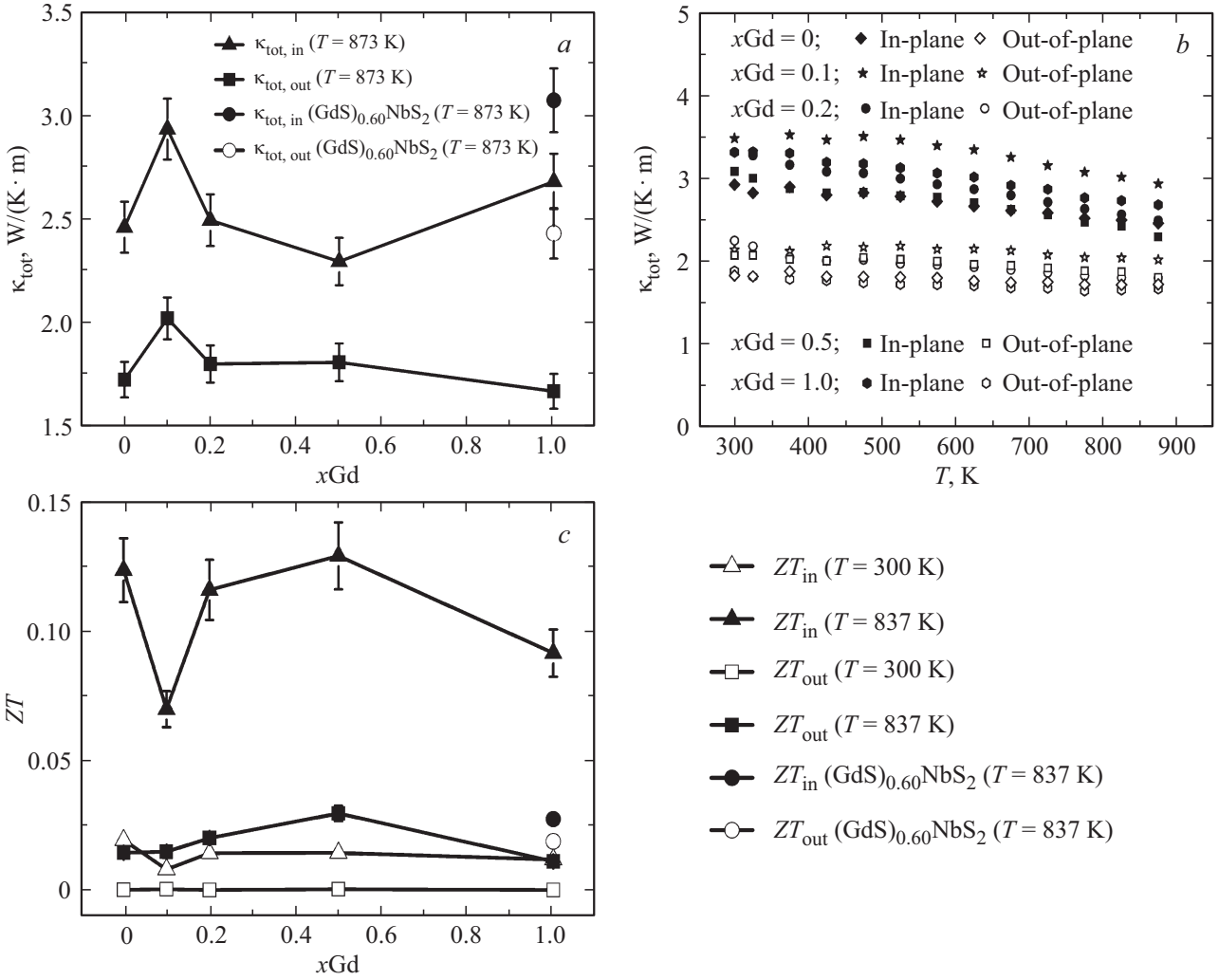

Figure 7. Dependencies of the thermal conductivity on xGd — (a), on temperature — (b) [25] and ZT parameters on the solid solution composition of xGd for $(GdS)_{1.20}NbS_2$, $(DyS)_{1.22}NbS_2$, $(Gd_{0.1}Dy_{0.9}S)_{1.21}NbS_2$, $(Gd_{0.2}Dy_{0.8}S)_{1.21}NbS_2$, $(Gd_{0.5}Dy_{0.5}S)_{1.21}NbS_2$, and $(GdS)_{0.60}NbS_2$ samples at 873 K — (c).

without $Dy^{(2\div3)+}$ ions the crystallites have larger sizes and disappears the disturbance of modulation of sublattice boundaries by parameters of unit cells a_1 and a_2 (the alternating modulation wave), which is typical for $(Gd_xDy_{1-x}S)$ disordered solid solutions. As a result, the thermal conductivity $\kappa_{tot,in}$ increases. However, the presence of a larger quantity of misfit modulated boundaries per unit volume between the [GdS] layer and the [NbS_2] single sandwich limits the increase in $\kappa_{tot,in}$.

For the $(GdS)_{0.60}NbS_2$ two-layer compound the number of lattice defects increases (Fig. 5, b), which is confirmed by a significant curving of the baseline in the Raman spectrum [29]. However, the volumetric density of modulated boundaries of sublattices is lower and therefore $\kappa_{tot,out}$ is considerably increased, and $\kappa_{tot,out,(GdS)_{0.60}NbS_2} > \kappa_{tot,out,(GdS)_{1.20}NbS_2}$. The comparison between $(GdS)_{1.20}NbS_2$ and two-layer $(GdS)_{0.60}NbS_2$ compounds has shown the difference between $\kappa_{tot,in,(GdS)_{1.20}NbS_2}$ and $\kappa_{tot,in,(GdS)_{0.60}NbS_2}$, when the temperature increases from 300 to 873 K. In addition, the anisotropy of $\kappa_{tot,(GdS)_{1.20}NbS_2}$ is higher than that of $\kappa_{tot,(GdS)_{0.60}NbS_2}$ (Fig. 7, a).

In the general case $\kappa_{tot} = \kappa_{lat} + \kappa_h$, where κ_{lat} — thermal conductivity of the lattice, and κ_h — thermal conductivity due to the drift of charge carriers (holes). In [25,50,53,54] values of κ_h were calculated for polycrystal samples using the Wiedemann–Franz law: $\kappa_h = L \cdot T \cdot \rho^{-1}$, where L — Lorentz number $(2.44 \cdot 10^{-8}\,W \cdot \Omega \cdot K^{-2})$. However, the use of the above-mentioned Lorentz number is justified for materials with certain properties. This number was derived theoretically for metals with free electrons within the framework of free gas model [54]. Then, with significant corrections, it was applied to semiconductors with parabolic bands [55]. At the same time, it was noted that the occurrence of boundaries within the main body of a sample introduces a significant uncertainty in the use of the Lorentz number. This matters, when there are a complex structure of bands and a complex energy dependence of the surface states relaxation time, as well as in the case of occurrence

of interband transitions or degeneracy removal at high temperatures [40,41,56,57].

It is known [58], that for an analog of the investigated misfit layer compounds, for example, $(LaS)_{1.14}NbS_2$, at 300 K the concentration of charge carriers is about $10^{21}\,cm^{-3}$ — the semiconductor is degenerated. If we take into consideration, that for nanostructured samples the conductivity can be limited by surface states on boundaries of crystallites, then it is clear that for $(Gd_xDy_{1-x}S)_zNbS_2$ compounds the use of classic Lorentz number for free electrons remains questionable.

To overcome these uncertainties, the following empirical expression was used:

$$L = 1.5 + \exp(-|S|/116) \qquad (6)$$

[23,54]. The use of this number has resulted in minor errors for some materials, including polycrystal ceramics [18,54]. However, for the compounds with solid solution lattices (alloys) the error in values of L can be as high as 25%. In addition, for materials with $S > 50\,\mu V \cdot K^{-1}$ the error in determining the value of L by equation (6) proposed in [57,59] can be 40%. In our case $S > 50\,\mu V \cdot K^{-1}$ at $T > 700$ K. If we take into consideration the above-mentioned surface and boundary changes in the chemical composition of crystallites in semiconductor ceramic polycrystal materials, then the use of the parabolic model as a prerequisite of operability of some above-mentioned options of L evaluation is not sufficiently justified [52,60].

Another variant of determining the lattice thermal conductivity of nanostructured materials κ_{lat} in relation to the thermal conductivity of the material without phonon scattering on defects with crystallites of macroscopic size κ_o is represented by the $\kappa_{lat} = (\kappa_o/3)(3l_{cr}/l_{Ph})$ function, where l_{cr} being crystallite size and l_{Ph} being length of free path of phonons [57], does not have a sufficiently clear justification for compounds with modulated boundaries of sublattices.

Thus, the use of equation: $\kappa_{tot} = \kappa_{lat} + \kappa_h$ to evaluate κ_{lat} and κ_h using known models of the Lorentz number selection in our and similar cases will result in a misinterpretation of the mechanisms of phonon scattering on the lattice and heat transfer by charge carriers. However, it can be assumed that $\kappa_{h,out}$ is very small because at 873 K $\rho_{out,(GdS)_{0.60}NdS_2} \gg \rho_{out,(GdS)_{1.20}NdS_2}$ and $\kappa_{tot,out,(GdS)_{0.60}NbS_2} > \kappa_{tot,out,(GdS)_{1.20}NbS_2}$. At the same time, since at 873 K $\rho_{in,(GdS)_{0.60}NbS_2} \sim \rho_{in,(GdS)_{1.20}NbS_2}$, and $\kappa_{tot,in(GdS)_{0.60}NbS_2} > \kappa_{tot,in(GdS)_{1.20}NbS_2}$, it can be assumed that $\kappa_{h,in}$ is small, but bigger than $\kappa_{h,out}$. Thus, the main mechanism of thermal conductivity is defined by the disturbances of short-range and long-range orders of the lattice and misfitting of lattice parameters of the [GdS] and $[NbS_2]$ subsystems.

Fig. 7, *c* shows dependencies of thermoelectric figure of merit (ZT) on the composition of investigated compounds. As before, we shall consider the change in these parameters with the change on composition xGd mainly at 873 K. As can be seen, values of ZT_{in} are considerably higher than those of ZT_{out}. In coordinates of $ZT-x$, the dependence is mirror opposite to the $CSR = f(x)$ dependence that characterize the disturbance of the long-range order of the crystal lattice (Fig. 5). Intervals of changes in S_{in} and ρ_{in} parameters with a change in concentration xGd are considerably less than those for S_{in}^2/ρ_{in} and $\kappa_{tot,in}$. In addition, the form of $S_{in}^2/\rho_{in} = f(x)$ and $ZT = f(x)$ dependencies is similar to that of the $N_{cr} = f(x)$ function.

All the considered effects give grounds to assume that the thermoelectric figure of merit ZT of pressed sintered misfit layer compounds $(Gd_xDy_{1-x}S)_zNbS_2$ is mainly defined by values of thermal conductivity and Seebeck coefficient. The highest values of ZT are achieved for samples with solid solutions $(Gd_xDy_{1-x}S)_{1.21}NbS_2$ at $x = 0.2$ and 0.5 (Fig. 7, *b*). For the $(GdS)_{0.60}NbS_2$ two-layer compound values of ZT are considerably lower and lie at a level of out-of-plane values for the $(GdS)_{1.20}NbS_2$ compound due to the increased thermal conductivity.

4. Conclusion

Using $(Gd_xDy_{1-x}S)_zNbS_2$ high-temperature compounds at temperatures of 300 and 873 K as an example, it is shown that a change in the composition of solid solution of the guest sublattice by replacement of one type of rare earth element ions by another — $[Gd_xDy_{1-x}S]$ allows controlling the disturbance of the short-range order of the crystal lattice due to the formation of a solution with different degree of disordering and long-range order due to a change in nanomorphology of crystallites. In the region of low concentrations ($x = 0.1$), the Gd^{3+} ions are concentrated as a SA on boundaries of crystallites and distributed mainly in the (028) plane forming a solid solution $[Gd_{0.1}Dy_{0.9}S]$ in this plane, which is close to an ordered solution. The Gd^{3+} ions concentrated on boundaries of crystallites are a SA and a promoter of the accelerated growth of crystallites. This is confirmed by an increase in size of D_{H-W} crystallites and a decrease in deformation stresses at $x = 0.1$. At the same time the degree of long-range order of the lattice increases. As a result, an anomalous change is observed in the thermoelectric parameters: S_{in} and ρ_{in} decrease by $\sim 10\%$, while $\kappa_{tot,in}$ increases by $\sim 25\%$, and ZT decreases by almost 2 times. In fact, the ZT changes in a similar way to the change in concentration of deformation centers N_{cr} on semicoherent boundaries of crystallites. With a decrease in size of crystallites in the interval of concentrations of xGd $= 0.1-0.5$, the short-range order of the lattice of intercalated layer $[Gd_xDy_{1-x}S]$ and the long-range order of the crystal lattice of compounds with misfit structure in general are disturbed. At the same time, the phonon structure of the investigated compounds becomes significantly more complex. This results in a decrease in thermal conductivity $\kappa_{tot,in}$, but causes insignificant changes in S_{in} and ρ_{iin} along the (006) basal plane. At the same time ZT increases up to 0.13 at 873 K. Thus, to increase values of ZT, it is necessary to decrease sizes of crystallites.

This is achieved through replacement of Dy^{3+} ions by Gd^{3+} ions in the whole volume of the sublattice of $[Gd_xDy_{1-x}S]$ solid solution with an excess concentration of SA of Gd^{3+} ions on boundaries of crystallites. It is noted, that to successfully improve efficiency of thermoelectric polycrystal ceramic materials, it is necessary to take into account crystal-chemical changes on boundaries of crystallites [47] and variations of modulated interfaces of sublattices [52,61], as well as the changes in electron structures related to them. To understand the nature of formation of thermo-emf and mechanisms of charges and heat transfer, including the heat transfer by charges, additional theoretical analyses of the effect of surface electron processes on boundaries of crystallites in polycrystal ceramic materials are needed.

The described scientific statements for $(Gd_xDy_{1-x}S)_{1.21}NbS_2$ compounds can be extended to other related nanostructured materials based on misfit layer compounds MTS_3 (M = Pb, Bi, Sn, Sb, rare earth elements and T = Ti, V, Cr, Nb, Ta) [14,17,18,28,30], and other layer compounds. It seems, that this study is a development of studies [21,61], where the effect of grain sizes, which are aggregates of crystallites, on the thermoelectric parameters of materials is considered.

Acknowledgments

The work was supported by the Ministry of Science and Higher Education of the Russian Federation, project No. 121031700315-2.

Conflict of interest

The authors declare that they have no conflict of interest.

References

[1] L.E. Bell. Science. **321**, *5895*, 1457 (2008).
[2] G. Tan, L.-D. Zhao, M.G. Kanatzidis. Chem. Rev. **116**, *19*, 12123 (2016).
[3] J.R. Sootsman, D.Y. Chung, M.G. Kanatzidis. Angew. Chem. Int. Ed. **48**, *46*, 8616 (2009).
[4] K. Nielsch, J. Bachmann, J. Kimling, H. Bottner. Adv. En. Mater. **1**, *5*, 713 (2011).
[5] M. Zebarjadi, K. Esfarjani, M.S. Dresselhaus, Z.F. Ren, G. Chen. Energy Envir. Sci. **5**, *1*, 5147 (2012).
[6] W.G. Zeier, A. Zevalkink, Z.M. Gibbs, G. Hautier, M.G. Kanatzidis, J.G. Snyder. Angew. Chem. Int. Ed. **55**, *24*, 6826 (2016).
[7] T. Zhu, Y. Liu, C. Fu, J.P. Heremans, J.G. Snyder, X. Zhao. Adv. Mater. **29**, *14*, 1605884 (2017).
[8] X. Su, P. Wei, H. Li, W. Liu, Y. Yan, P. Li, C. Su, C. Xie, W. Zhao, P. Zhai, Q. Zhang, X. Tang, C. Uher. Adv. Mater. **29**, 1602013 (2017).
[9] M. Ohta, P. Jood, M. Murata, C.-H. Lee, A. Yamamoto, H. Obara. Adv. Mater. **9**, 1801304 (2019).
[10] J.G. Snyder, E.S. Toberer. Nature Mater. **7**, *2*, 105 (2008).
[11] G.A. Slack. CRC Handbook of thermoelectrics. (1995). P. 407–440.
[12] G.S. Nolas, D.T. Morelli, T.M. Tritt. Annu. Rev. Mater. Sci. **29**, 89 (1999).
[13] T. Takabatake, K. Suekini, T. Nakayama, E. Kaneshita. Rev. Mod. Phys. **86**, *2*, 669 (2014).
[14] G.A. Wiegers. Prog. Solid State Chem. **24**, 1 (1996).
[15] P. Jood, M. Ohta, O.I. Lebedev. Chem. Mater. **27**, *22*, 7719 (2015).
[16] V.V. Sokolov, V.V. Bakovetz, S.M. Luguev, N.V. Lugueva. Adv. Mater. Phys. Chem. **2**, 25 (2012).
[17] Y. Miyazaki, H. Ogawa, T. Nakajo, Y. Kikuchii, K. Hayashi. J. Electron. Mater. **42**, 1335 (2013).
[18] K. Biswas, J. He, I.D. Blum, C.-I. Wu, T.P. Hogan, D.N. Seidman, V.P. Dravid, M.G. Kanatzidis. Nature. **489**, *7416*, 414 (2012).
[19] V.A. Kulbachinsky, Ros. nanotekhnologii **14**, *7–8*, 30 (2019) (in Russian)
[20] D.K. Aswal, R. Basu, A. Singh. Energy Conv. Manag. **114**, 50 (2016).
[21] Y.-P. Wang, B.-C. Qin, D.-Y. Wang, T. Hong, X. Gao, L.-D. Zhao. Rare Met. **40**, *2*, 2819 (2021).
[22] A.V. Sotnikov, V.V. Bakovets, A.Sh. Agazhanov, S.V. Stankus, D.P. Pichshur, V.V. Sokolov, FTT **60**, *3*, 482 (2018) (in Russian).
[23] S.J. Gomez, D. Cheikh, T. Vo, P.V. Allmen, K. Lee, M. Wood, G.J. Snyder, B.S. Dunn, J.-P. Fleurial, S.K. Bux. Chem. Mater. **31**, 4460 (2019).
[24] V.V. Bakovets, A.V. Sotnikov, A.Sh. Agazhanov, S.V. Stankus, E.V. Korotaev, D.P. Pishchur, A.I. Shkatulov. J. Am. Ceram. Soc. **101**, *10*, 4773 (2018).
[25] A.V. Sotnikov, M. Ohta, P. Jood. ACS Omega. **5**, *22*, 13006 (2020).
[26] A. Meerschaut, P. Rabu, J. Rouxel. J. Solid State Chem. **78**, *1*, 35 (1989).
[27] R. Roesky, A. Meerschaut, P. Gressier, J. Rouxel. MRS Bull. **29**, *9*, 943 (1994).
[28] A. Jobst, S. Van Smaalen. Acta Cryst. **58**, 179 (2002).
[29] A.V. Sotnikov, V.V. Bakovets, E.V. Korotaev, S.V. Trubina, V.I. Zaikovskiy. Mater. Res. Bull. **131**, 110963 (2020).
[30] S. Van Smaalen. J. Phys. Condens. Mater. **3**, *10*, 1247 (1991).
[31] R.D. Shannon, C.T. Prewitt. Acta Crystallogr. Sect. B. **25**, *5*, 925 (1969).
[32] R.A. Svelin, Termodinamika tverdogo sostoyaniya, Metallurgiya, M., (1968), 314 p. (in Russian).
[33] Zh. Fridel', Dislokatsii. Mir, M., (1967), 643 p. (in Russian).
[34] G.K. Williamson, R.E. Smallman. Phil. Mag. **1**, *1*, 34 (1956).
[35] A.L. Patterson. Phys. Rev. **56**, 978 (1939).
[36] G.K. Williamson, W.H. Hall. Acta Met. **1**, *1*, 22 (1953).
[37] Ch. Kittel, Elementarnaya fizika tverdogo tela, Nauka, M., (1965), 369 p. (in Russian).
[38] L.D. Landau, E.M. Lifshitz, Teoriya uprugosti, Nauka, M. (1987), 248 p. (in Russian)
[39] H.J. Goldsmid, F.A. Underwood. Adv. En. Conv. **7**, *4*, 297 (1968).
[40] B.M. Gol'tsman, V.A. Kudimov, I.A. Smirnov, Poluprovodnikovye termodinamicheskiye materialy na osnove Bi_2Te_3, Nauka, M., (1972), 320 p. (in Russian).
[41] I.A. Smirnov, V.I. Tamarchenko, Elektronnaya teploprovodnost' v metallakh i poluprovodnikakh, Nauka, L., (1977). 151 p. (in Russian).
[42] J. Rouxel, Y. Moëlo, A. Lafond, F.J. Di Salvo, A. Meerschaut, R. Roesky. Inorg. Chem. **33**, *15*, 3358 (1994).

[43] K. Suzuki, T. Enoki, K. Imaeda. Solid State Commun. **78**, *2*, 73 (1991).
[44] T. Terashima, N. Kojima. J. Phys. Soc. Jpn. **63**, 658 (1994).
[45] K. Suzuki, T. Kondo, T. Enoki. Synthetic Met. **55**–**57**, 1741 (1993).
[46] O. Pena, P. Rabu, A. Meerschaut. J. Phys. Condens. Mater. **3**, 9929 (1991).
[47] K.V. Shalimova, Fizika poluprovodnikov. Energoatomizdat, M. (1985), 392 p. (in Russian).
[48] K.A. Jackson, W. Shroter. Hadbook of semiconductor technology. Wiley-VCH, (2000). 829 p.
[49] H. Statz, G.A. Demars, L. Davis, A. Adams. Phys. Rev. **101**, *4*, 1272 (1956).
[50] C.B. Vining. J. Appl. Phys. **69**, *1*, 331 (1991).
[51] J. He, M.G. Kanatzidis, V.P. Dravid. Mater. Today. **16**, *5*, 166 (2013).
[52] B. He, Y. Wang, M.Q. Arguilla, N.D. Cultrara, M.R. Scudder, J.E. Goldberger, W. Wind, J.P. Heremans. Nature Mater. **18**, 568 (2019).
[53] T. Deng, T. Xing, M.K. Brod, Y. Sheng, P. Qiu, I. Energy Envir. Sci. **13**, *9*, 3041 (2020).
[54] H-S. Kim, Z.M. Gibbs, Y. Tang, H. Wang, G.J. Snyder. Appl. Mater. **3**, *4*, 041506 (2015).
[55] E.D. Devyatkova, I.A. Smirnov. Solid State Chem. **3**, *8*, 2310 (1961).
[56] L.P. Bulat, I.A. Drabkin, V.V. Karataev, V.B. Osvenskii, D.A. Pshenai-Severin. Phys. Solid State **52**, *9*, 1836 (2010).
[57] J.W. Sharp, S.J. Poon, H.J. Goldsmid. Phys. Status Solidi A. **187**, *2*, 507 (2001).
[58] P. Jood, M. Ohta, H. Nishiate, A. Yamamoto, O.I. Lebedev, D. Berthebaud, K. Suekuni, M. Kunii. Chem. Mater. **26**, *8*, 2684 (2014).
[59] E.S. Toberer, L.L. Baranowski, C. Dames. Annu. Rev. Mater. Res. **42**, *20*, 179 (2012).
[60] I.A. Smirnov, B.Ya. Moizes, E.D. Devijtkova, E.D. Nensberg, A.A. Averkin. Proc. Int. Conf. Semicond. Phys. (1960). 645 p.
[61] I.S. Flyagina, A.A. Petrov, V.S. Pervov, Uspekhi khimii **85**, *6*, 610618 (2016) (in Russian).

Translated by Ego Translating